TiO_2-Reinforced Alginate-Acrylic-Itaconic Acid Hydrogel for Efficient Brilliant Green Adsorption

Uday Abdul-Reda Hussein[1], Ali Fawzi Al-Hussainy[2], Wasam Naj[3], Alzahraa S. Abdulwahid[4], Hadil Hussain Hamza[5], Aseel M. Aljeboree[6], and Ayad F. Alkaim[6,*]

[1]Department of pharmaceutics, College of Pharmacy, University of Al-Ameed, Iraq
[2]College of Pharmacy, Ahl Al Bayt University, Kerbala, Iraq
[3]Al-Manara College For Medical Sciences, Maysan, Iraq
[4]Al-Hadi University College, Baghdad, Iraq
[5]Department of Medical Laboratories Technology, Al-Nisour University College, Nisour Seq. Karkh, Baghdad, Iraq
[6]Department of Chemistry, College of Science for Women, University of Babylon, Hilla, Iraq
Email: ud.rikaby@alameed.edu.iq (U.A.-R.H.); Ali.Faowzy2.1991@gmail.com (A.F.A.-H.); wasam.lab@uomanara.edu.iq (W.N.); mszahrasabah@huc.edu.iq (A.S.A.); Hadeel.path@nuc.edu.iq (H.H.H.); annenayad@gmail.com(A.M.A.); alkaimayad@gmail.com (A.F.A.)
*Corresponding author

Manuscript received September 2, 2025; revised February 5, 2026; accepted March 2, 2026; published June 25, 2026.

***Abstract*—This study introduces a novel hydrogel design in which the combined incorporation of itaconic acid and Titanium dioxide (TiO_2) nanoparticles into an alginate–acrylic matrix creates a synergistic structure with enhanced functional groups, improved stability, and superior adsorption performance. This dual organic–inorganic modification distinguishes the material from conventional hydrogels and represents a meaningful advancement in dye-removal hydrogel systems. A Sodium Alginate (SA) based hydrogel was synthesized through free-radical copolymerization of Acrylic Acid (AA) and Itaconic Acid (IA), followed by incorporation of TiO_2 nanoparticles as functional and reinforcing additives. The structure of the SA-g-(AA-co-IA)/TiO_2 hydrogel was confirmed by Scanning Electron Microscopy (SEM), X-Ray Diffraction (XRD), and Thermogravimetric Analysis (TGA). SEM revealed a porous network with uniformly distributed TiO_2 nanoparticles, while XRD indicated a semi-crystalline matrix retaining TiO_2 crystalline phases. TGA showed improved thermal stability in TiO_2-loaded hydrogels. The material exhibited strong swelling behavior, reaching up to 800% of its dry weight, and demonstrated clear pH-responsive properties. In dye-removal tests, pristine TiO_2 showed low adsorption, whereas the composite hydrogel achieved a 91.2% removal efficiency for Brilliant Green (BG), significantly outperforming the unloaded hydrogel (73.4%). Isotherm analysis indicated that the adsorption followed the Freundlich model, indicating multilayer adsorption. The maximum adsorption capacity (Q_m = 162.22 mg/g) indicated strong interactions between BG molecules and the hydrogel surface. These results highlight the synergistic role of TiO_2 NPs and the copolymer network in enhancing adsorption performance. The developed hydrogel represents a promising multifunctional material for wastewater treatment and other stimuli-responsive applications.**

***Keywords*—acrylic-itaconic acid, Titanium dioxide, brilliant green, pH-responsive hydrogel, biopolymer nanocomposite**

I. Introduction

Environmental contamination, particularly the release of organic and inorganic pollutants into aquatic systems, has become a major global challenge driven by rapid industrial expansion and urbanization. Conventional treatment processes such as chemical precipitation, membrane filtration, and biological degradation often suffer from high operating costs, limited selectivity, or poor efficiency at low pollutant concentrations. Consequently, adsorption has emerged as a preferred alternative due to its simplicity, low cost, reusability, and high removal efficiency [1–5].

Hydrogels are three-dimensional polymeric networks that can retain large volumes of water while maintaining structural integrity. Their biocompatibility, tunable chemical functionality, and responsiveness to external stimuli make them promising candidates for wastewater treatment [6–8]. Natural polysaccharides—particularly Sodium Alginate (SA)—have attracted significant interest because of their biodegradability, availability of reactive hydroxyl and carboxyl groups, and strong gel-forming ability. Synthetic monomers, such as Acrylic Acid (AA), further enhance hydrogel swelling, pH responsiveness, and ion-exchange capacity. In contrast, bio-derived Itaconic Acid (IA) introduces additional carboxyl groups, thereby improving hydrophilicity, mechanical strength, and pollutant-binding capacity [9–11].

Although numerous SA-based hydrogels and AA/IA copolymer systems have been reported, their adsorption capacity remains limited by poor mechanical stability, low surface area, or insufficient active sites. Moreover, only a few studies have explored the incorporation of inorganic nanoparticles into SA-g-poly (acrylic/itaconic) matrices [12, 13]. Titanium dioxide (TiO_2) nanoparticles, in particular, offer high stability, hydrophilicity, and abundant surface hydroxyl groups, yet their synergistic interaction with an SA-AA-IA hydrogel network has not been systematically investigated. This represents a clear gap in current literature regarding how TiO_2 reinforcement may enhance swelling behavior, structural robustness, and adsorption efficiency [7, 14–18].

In this context, the present study reports the synthesis of a novel SA-g-(AA-co-IA)/TiO_2 composite hydrogel prepared via free-radical copolymerization. The hydrogel is designed to combine the biodegradability of SA, the pH-responsive swelling of AA, the multifunctional binding sites of IA, and the structural reinforcement of TiO_2 nanoparticles. Comprehensive physicochemical and adsorption studies are conducted to evaluate its potential as an efficient and environmentally friendly adsorbent for water decontamination.

II. Experimental Part

A. Preparation of the Composite Hydrogel

A TiO_2-reinforced composite hydrogel was synthesized via free-radical copolymerization using Sodium Alginate (SA), Acrylic Acid (AA), and Itaconic Acid (IA). Sodium alginate (2.0 g; ≈10.1 mmol) was dissolved in 20 mL of deionized water at 40 °C to obtain a 2 wt% solution. Separately, AA (10 mL; 10.51 g; 145.8 mmol) and IA (2 mL; 3.26 g; 25.0 mmol) were mixed with 3 mL of water, followed by the addition of potassium persulfate (KPS, 0.10 g; 0.37 mmol) as the initiator and N,N′-Methylene Bisacrylamide (MBA, 0.05 g; 0.32 mmol) as the cross-linker. Titanium dioxide nanoparticles (0.20 g; ~25 nm) were incorporated into the monomer mixture and ultrasonicated for 10 min to ensure uniform dispersion. The SA solution was gradually introduced into the monomer–TiO_2 phase under vigorous stirring to produce a homogeneous precursor, which was then cast into Petri dishes and thermally polymerized at 60 °C for 1.5 h. Gelation occurred within 30–45 min, yielding a stable hydrogel network. The resulting hydrogel was repeatedly washed with deionized water to remove unreacted species, aged for 24 h at room temperature, and dried at 55 °C to a constant weight before further characterization. As shown in Fig. 1.

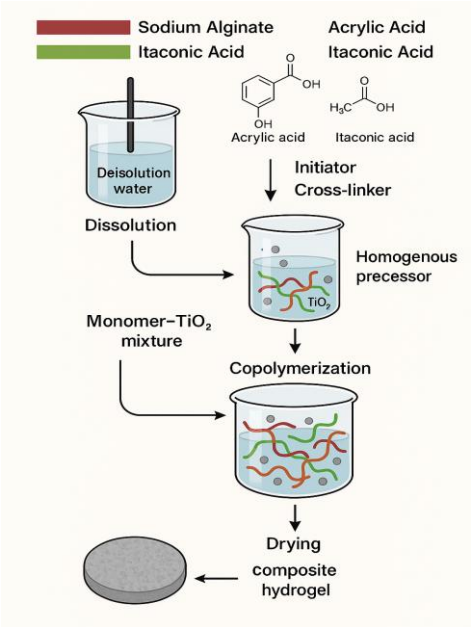

Fig. 1. Preparation of SA/AA-IA-based hydrogel incorporating TiO_2 NP_S via free radical polymerization.

B. Adsorption of BG Dye from Aqueous Solution

Batch adsorption experiments were conducted to investigate the removal of BG, a basic dye, from aqueous solutions. In each experiment, 100 mL of BG dye solution with an initial concentration of 100 mg/L was placed in a 100 mL conical flask. Adsorption doses of hydrogel (0.08 g) were used as the adsorbent. The flasks were placed in a shaking water bath and agitated at 200 rpm for 1 h to facilitate adsorption. After the adsorption period, the mixtures were removed from the shaker and centrifuged to separate the solid and liquid phases. The residual dye concentration in the supernatant was measured using a UV-Vis spectrophotometer (Shimadzu UV-1800) at a maximum wavelength (λmax) of 599 nm, corresponding to BG dye. The adsorption efficiency (Q_e, mg/g), percentage removal (R%) were calculated using standard adsorption equations (Eqs. (1) and (2)).

$$Q_e = \frac{(C_o - C_e)V}{M} \quad (1)$$

$$E\% = \frac{C_o - C_e}{C_o} \times 100\% \quad (2)$$

where C_0 and C_e (mg/L) represent the initial and equilibrium concentrations of the BG dye, respectively M(g) is the mass of the hydrogel adsorbent, and V(L) is the volume of the dye solution [19].

C. Swelling Ratio

The swelling behavior of the SA-g-(AA-co-IA)/TiO_2 hydrogel was assessed in distilled water to determine its Swelling Ratio (SR%). A dried hydrogel sample (0.05 g) was immersed in 200 mL of distilled water at room temperature. At 60-Minute intervals, the sample was removed, gently blotted with filter paper to eliminate surface moisture, and weighed. The SR% was calculated using Eq. (3) based on the difference between the hydrogel's dry mass and swollen mass.

$$(SR\%) = \frac{M(swollen) - M(dry)}{M(dry)} \times 100\% \quad (3)$$

III. Results and Discussion

The Scanning Electron Microscopy (SEM) micrograph of the SA-g-(AA-co-IA)/TiO_2 hydrogel (Figs. 2a and 2b) reveals a highly porous, anisotropic morphology composed of aligned fibrous structures. The presence of uniformly distributed spherical and irregular TiO_2 nanoparticles is evident from the brighter high-contrast regions, confirming successful nanoparticle incorporation within the polymer matrix. The nanoscale roughness and interconnected porosity indicate an enlarged effective surface area, consistent with the observed BET mesoporosity. Such features are favorable for adsorption and enhanced interfacial interactions due to the abundant carboxyl and hydroxyl groups originating from AA and IA [20].

A. X-Ray Diffraction (XRD) Interpretation of SA-g-(AA-co-IA)/TiO_2 Hydrogel

The XRD pattern of the TiO_2-reinforced hydrogel composite exhibits a broad diffraction halo centred around 20–25° without distinct Bragg reflections Fig. 3. This behavior is attributed primarily to the amorphous nature of the polymeric network formed via free-radical copolymerization of sodium alginate, acrylic acid, and itaconic acid. Such crosslinked hydrogel systems inherently lack long-range crystalline order, resulting in diffuse scattering rather than sharp diffraction peaks. Although TiO_2 nanoparticles are crystalline in their native state, their relatively low loading (≈1–2 wt%) within the composite, combined with their homogeneous nanoscale dispersion throughout the polymer matrix, significantly reduces their

diffraction intensity. Furthermore, the strong amorphous background generated by the hydrogel matrix overlaps with the characteristic TiO_2 reflections (particularly near 25°), effectively masking weak crystalline signals.

It is well documented that, in polymer–nanoparticle composites, low filler content and high dispersion can suppress or broaden nanoparticle diffraction peaks due to reduced coherent scattering domains and matrix-induced attenuation. Therefore, the absence of sharp TiO_2 peaks in the composite XRD pattern does not indicate the absence of nanoparticles, but rather reflects their low concentration and effective incorporation within an amorphous three-dimensional network [21, 22].

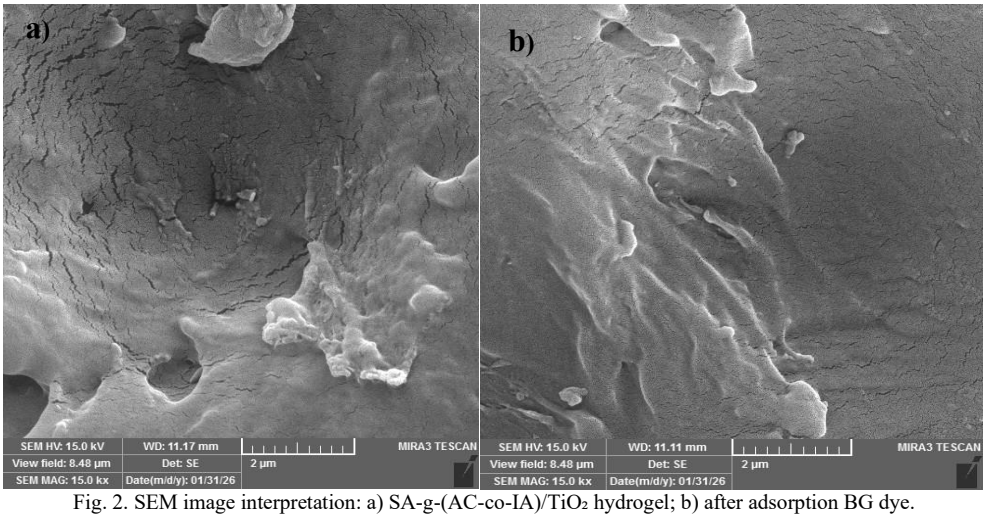

Fig. 2. SEM image interpretation: a) SA-g-(AC-co-IA)/TiO_2 hydrogel; b) after adsorption BG dye.

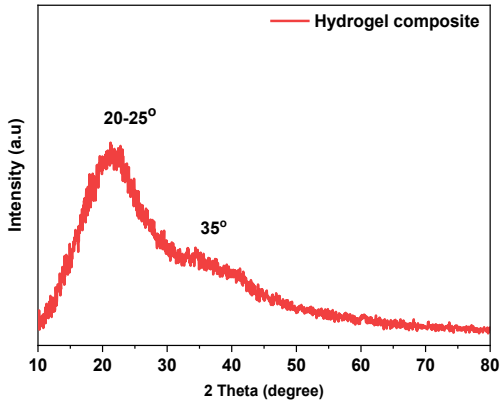

Fig. 3. XRD analysis of SA-g-(AA-co-IA)/TiO_2 hydrogel.

B. BET Analysis and Isotherm Interpretation of TiO_2-Loaded Hydrogel

The nitrogen adsorption–desorption isotherm of the SA-g-(AA-co-IA)/TiO_2 hydrogel exhibited a clear Type IV profile with an H_3 hysteresis loop according to the IUPAC classification, confirming the presence of a mesoporous structure. The hysteresis behavior is characteristic of slit-shaped pores or non-rigid aggregates, typically observed in layered or plate-like materials. Quantitative BET analysis revealed a specific surface area of 56.3 m^2/g, a total pore volume of 0.142 cm^3/g, and an average pore diameter of 10.1 nm, situating the hydrogel firmly within the mesopore regime (2–50 nm) (in Fig. 4). These parameters collectively indicate that incorporating TiO_2 enhances both the accessible surface area and the pore architecture, providing a moderately high surface area and well-defined mesoporosity. Such characteristics are advantageous for adsorption-based applications, as they facilitate improved molecular diffusion and increased availability of active sites, thereby enhancing the hydrogel's functional performance [21–23].

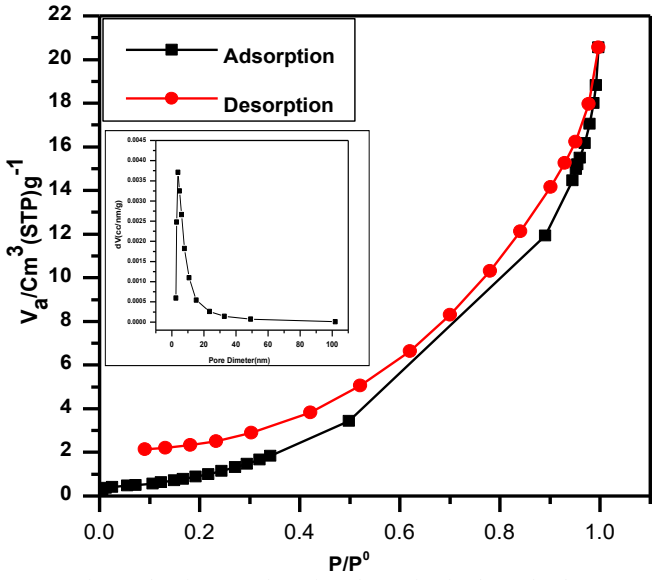

Fig. 4. The nitrogen adsorption–desorption isotherm for the SA-g-(AC-co-IA)/TiO_2 hydrogel.

C. TEM Analysis of Hydrogel and Hydrogel Composite

The TEM image of the SA-g-(AA-co-IA) hydrogel (Fig. 5a) shows a semi-transparent, amorphous morphology with low electron-density contrast, typical of organic polymer networks lacking inorganic fillers. The sheet-like structure with non-uniform thickness indicates a soft, disordered hydrogel matrix formed by alginate, acrylic acid, and itaconic acid. The absence of dark contrast regions confirms the lack of inorganic nanoparticles and supports the amorphous character observed in the XRD results [24].

In contrast, the TEM micrograph of the TiO_2-loaded hydrogel (Fig. 5b) exhibits a denser structure with distinct dark regions corresponding to TiO_2 nanoparticles. These high-electron-density zones demonstrate successful

incorporation of TiO_2 within the polymer matrix. The nanoparticles appear well distributed and embedded, indicating good interfacial compatibility between TiO_2 and the hydrogel chains. Compared to the pristine hydrogel, the composite shows enhanced structural definition, reflecting the reinforcing effect of the inorganic filler [25, 26].

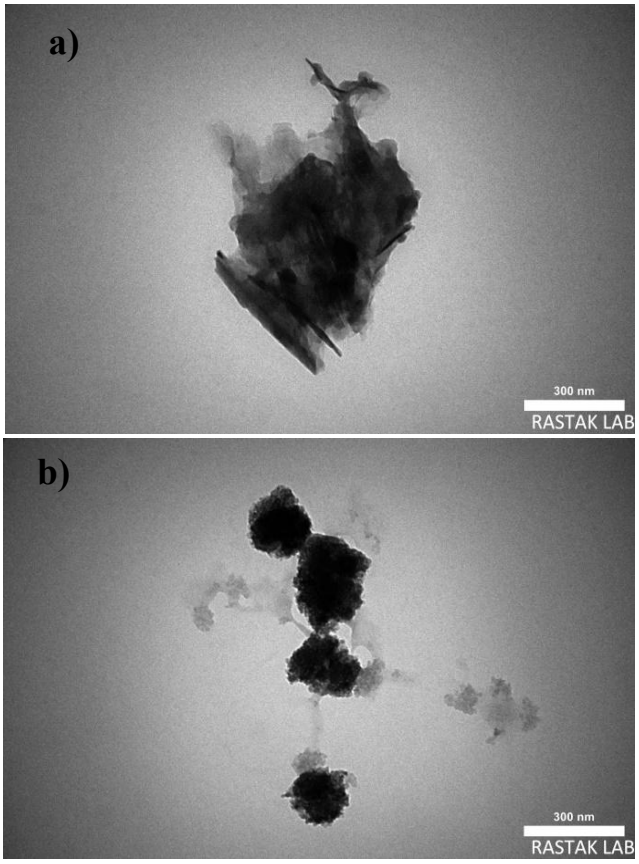

Fig. 5. TEM analysis; a) SA-g-(AC-co-IA); b) SA-g-(AC-co-IA)/TiO_2 hydrogel.

D. Thermal Stability Analysis of SA-g-(AC-co-IA)/TiO_2 Hydrogel

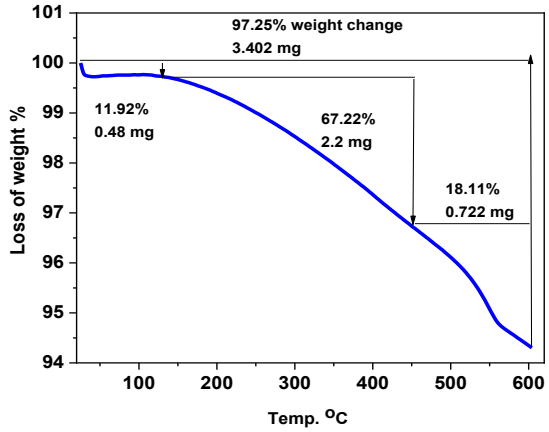

Fig. 6. Thermal Stability Analysis of SA-g-(AC-co-IA)/TiO_2 Hydrogel.

The Thermogravimetric Analysis (TGA) curve of the SA-g-(AA-co-IA)/TiO_2 hydrogel (Fig. 6) exhibits a multistep thermal degradation pattern. A minimal mass change is observed below 100 °C, corresponding to the evaporation of physically adsorbed water. Between 100 and 500 °C, the hydrogel undergoes gradual decomposition of its organic components, including the alginate backbone and the side chains of acrylic and itaconic acids. The slow, steady weight loss in this region reflects the stabilizing effect of TiO_2, which enhances the thermal resistance of the polymer network. A more pronounced mass loss beyond 500 °C is associated with carbonization and the breakdown of residual polymer fragments. The overall mass loss is relatively low (~6% at 600 °C), indicating that the composite possesses good thermal stability due to strong crosslinking and the reinforcing contribution of the inorganic TiO_2 phase [7, 26].

E. Factors that Affect the Swelling Ratio of the Hydrogel

1) Influence of temperature on the swelling response

The swelling ratio (SR%) of the hydrogel was significantly affected by the temperature of the swelling medium, as depicted in Fig. 7. As the temperature increased from 40 to 70 °C, the SR% increased gradually, reaching a maximum around 70 °C. This enhancement in SR can be attributed to the greater mobility of polymer chains and to the swelling of the hydrogel network at high temperatures, which allows the hydrogel to absorb water more effectively [27, 28].

A rapid decrease in the swelling ratio was observed after heating to 70 °C, which could be attributed to either partial compaction or thermal shrinkage of the hydrogel network, possibly due to the loss of hydrogen bonds or to polymer chain contraction. When the temperature was increased to 90 °C, it demonstrated reduced swelling due to system collapse or dehydration at high temperatures. It appears that the hydrogel exhibits temperature-sensitive swelling behavior and may have an optimum temperature for maximum water absorption in the range of 60–70 °C [29, 30].

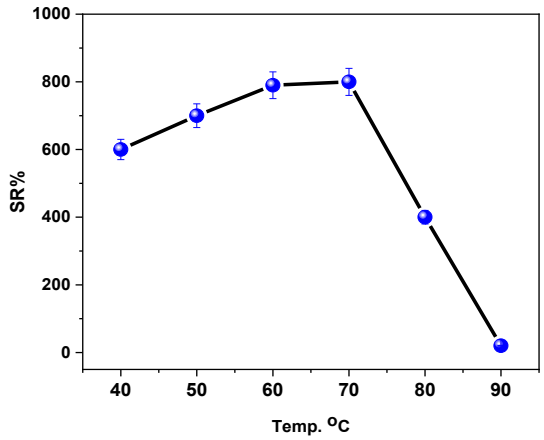

Fig. 7. Effect of temperature on the swelling response of the SA-g-(AC-co-IA)/TiO_2 hydrogel.

2) pH-responsive swelling property for the hydrogel

The swelling behavior of the SA-g-(AA-co-IA)/TiO_2 hydrogel exhibits a pronounced pH-dependent response (Fig. 8). At acidic conditions (pH 2–4), the hydrogel shows minimal swelling because the carboxylic groups (–COOH) within the network remain predominantly protonated. Under these conditions, electrostatic repulsion between polymer chains is negligible, resulting in a compact, tightly collapsed structure that limits water uptake. As the pH increases above 5, the carboxyl groups progressively ionize to $–COO^-$, generating higher intramolecular charge density [12, 31]. This ionization enhances electrostatic repulsion and increases the osmotic pressure inside the network, consistent with the

Flory-Rehner swelling theory, resulting in substantial expansion of the hydrogel matrix [32]. The swelling ratio reaches its maximum in alkaline media (pH 10–12), where most ionizable groups are fully deprotonated, producing a highly extended polymer network. The plateau observed at high pH indicates that the hydrogel has reached its equilibrium swelling capacity, where further increases in pH do not significantly enhance chain repulsion or water absorption [30, 33].

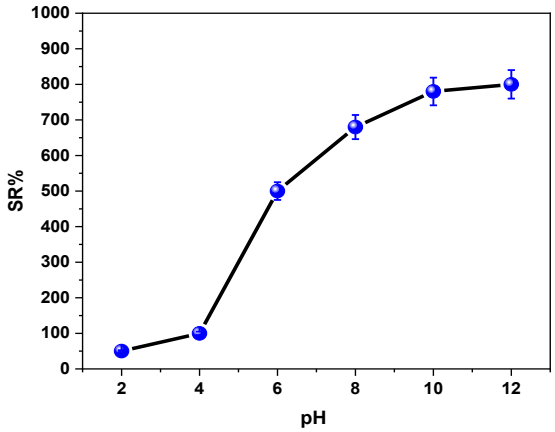

Fig. 8. Effect of pH-Responsive Swelling Property for the SA-g-(AC-co-IA)/TiO_2 Hydrogel.

3) Influence of contact time on the swelling ratio of SA-g-(AC-co-IA)/TiO_2 hydrogel

The swelling dynamics of the SA-g-(AC-co-IA)/TiO_2 hydrogel were investigated as a function of time of contact in distilled water. As illustrated in Fig. 9, the swelling ratio (SR%) gradually increased over time, demonstrating a rapid water absorption within the first hours. Such rapid swelling behaviour can primarily be ascribed to the high content of hydrophilic functional groups (–COOH and –OH) in the hydrogel matrix, which readily form hydrogen bonds with water molecules [20, 34].

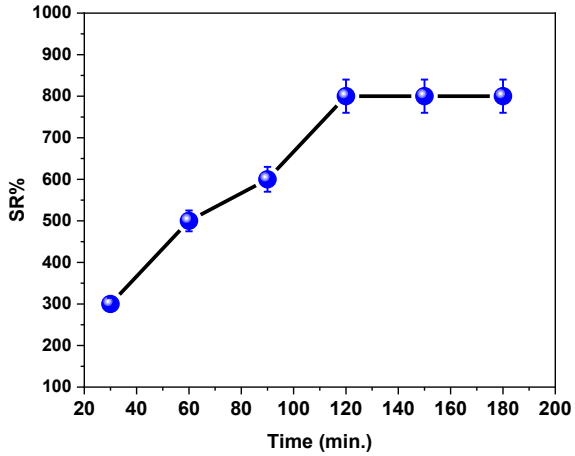

Fig. 9. Influence of contact time on the swelling ratio of SA-g-(AC-co-IA)/TiO_2 hydrogel.

The swelling ratio continued to increase over time, reaching a plateau after 120 min, indicating that the hydrogel network had attained its maximum swelling and reached equilibrium. Above this value, the swelling does not increase substantially, indicating saturation of the free volume in the hydrogel's structure. The presence of TiO_2 nanoparticles could promote a more porous, crosslinked network, facilitating water diffusion at the initial stages but impeding further expansion after reaching equilibrium. These results demonstrate that the hydrogel has time-dependent swelling behavior and reaches equilibrium within 2 h under the present conditions [22, 35].

F. Effect of Different Parameters Affecting Adsorption

1) Effect of contact time

Hydrogel Composite (black squares): Shows the fastest and highest removal efficiency, reaching ~50% in the first 5 min and ~95% at 30 min. Reaches equilibrium quickly, indicating abundant active sites and a high adsorption affinity. Hydrogel (red circles): Moderate adsorption rate, reaching ~20% at 5 min and ~80% after ~35–40 min. Slower kinetics than the composite but still significantly better than TiO_2 NPs, suggesting good porosity and active functional groups [36]. TiO_2 Nanoparticles (blue triangles): Lowest performance, with a maximum of ~23% removal even after 35 min. Limited adsorption due to a small number of active adsorption sites—mainly suited for photocatalytic rather than pure adsorption processes. Comparison of Results: Hydrogel composite > Hydrogel > TiO_2 NPs. The hydrogel composite outperforms due to the combined advantages of the hydrogel's adsorption capacity and TiO_2's surface properties, enabling faster kinetics and higher equilibrium removal [37], as shown in Fig. 10.

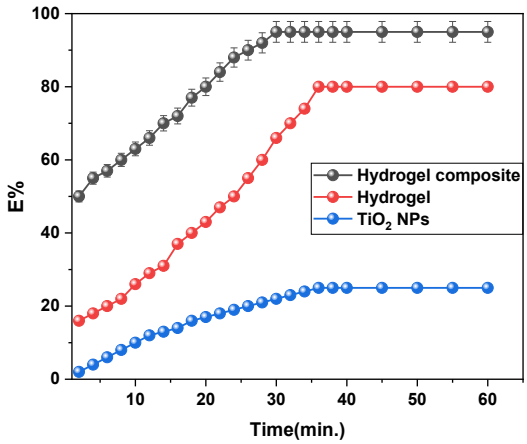

Fig. 10. Effect of contact time of hydrogel composite, hydrogel and TiO_2 NPs on the removal of BG dye (adsorption dose 0.08 g, conc. 100 mg/L, pH 7, T 25 °C).

2) Effect of pH

The pH-dependent adsorption trends (Fig. 11) reveal fundamental differences in the surface chemistry and interaction mechanisms of the three adsorbents. Bare TiO_2 nanoparticles show minimal variation in removal efficiency (≈ 10–15 %) across the entire pH range, which is consistent with earlier studies showing that non-modified TiO_2 exhibits poor affinity toward cationic dyes under dark conditions due to its near-neutral surface charge and limited density of accessible binding sites. This confirms that TiO_2 alone is not an effective adsorbent for BG dye [38].

In contrast, the SA-g-(AA-co-IA) hydrogel demonstrates a much stronger pH response, increasing from ~20% removal at pH 2 to ~88% at pH 10. This behavior aligns with polyacid ionization theory, where deprotonation of –COOH groups

above their pKa enhances the negative charge density and thereby strengthens electrostatic attraction toward cationic dyes. Similar pH-responsive swelling and adsorption behavior has been reported for acrylic-based hydrogels, supporting the mechanistic explanation [39].

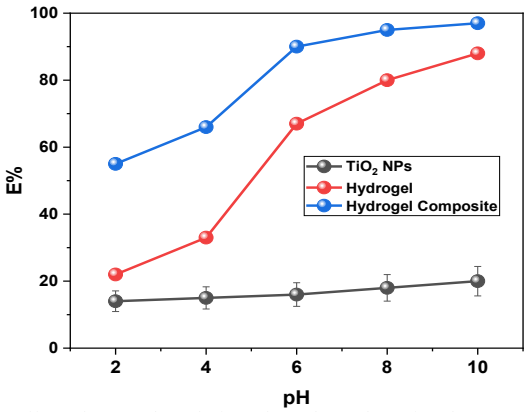

Fig. 11. Effect of pH on the solution of BG dye (adsorption dose 0.08 g, conc. 100 mg/L, T 25 ℃, contact Time 60 min).

The hydrogel composite shows the highest pH sensitivity, rising from ~55% at pH 2 to nearly 100% at pH 10. The steep improvement compared with the pristine hydrogel indicates a real synergistic effect, not just additive behaviour. TiO_2 incorporation increases the density of Lewis acidic/negative surface sites, improves water uptake, and enhances pore stability, all of which promote dye-matrix interactions. Comparable TiO_2-alginate composites reported in the literature typically achieve 70–90% removal, but the near-quantitative removal observed here highlights the improved performance of the present system [40]. This demonstrates that integrating TiO_2 within the AA-IA-alginate network produces a composite with stronger pH-responsive charge modulation and superior adsorption efficiency, representing a notable advancement beyond conventional alginate hydrogels.

G. Adsorption Efficiency Comparison for BG Dye

The competitive adsorption study (Fig. 12) clearly shows a performance hierarchy among the three adsorbents. Bare TiO_2 nanoparticles gave the lowest BG removal (18.7%), which is consistent with reports that unsupported TiO_2 has limited adsorption capacity and weak interaction with organic dyes in the absence of photonic activation [38]. In contrast, the SA-g-(AA-co-IA) hydrogel removed 73.4% of BG, owing to its porous network and the high density of ionizable –COOH/–OH groups that generate electrostatic attraction toward cationic dyes. Similar behaviour has been reported for acrylic-acid–grafted alginate hydrogels used for cationic dye removal [38]. The SA-g-(AA-co-IA)/TiO_2 hydrogel achieved the highest efficiency (91.2%), demonstrating a clear synergistic effect between the polymer matrix and the inorganic filler. This improvement is in line with other TiO_2-reinforced alginate hydrogels, which show enhanced adsorption (often > 90%) and improved structural stability compared with the polymer or TiO_2 alone [40]. These results confirm that the designed composite is more effective for BG removal than either constituent alone and compares favourably with previously reported TiO_2-alginate systems [22].

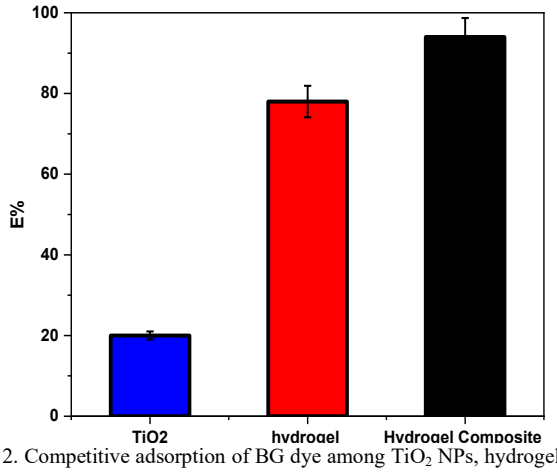

Fig. 12. Competitive adsorption of BG dye among TiO_2 NPs, hydrogel, and hydrogel composite (adsorption dosage 0.08 g, conc. 100 mg/L, pH 7, and contact time 60 min).

H. Regeneration and Reuse

The regeneration performance of the adsorbents over five adsorption-desorption cycles is presented in Fig. 13. The hydrogel composite demonstrated the highest stability, retaining approximately 80% of its initial removal efficiency after five cycles, compared to ~58% for the pristine hydrogel and < 20% for TiO_2 nanoparticles alone. This enhanced reusability is attributed to the strong cross-linked network provided by the SA-g-(AA-co-IA) matrix and the structural reinforcement imparted by TiO_2 nanoparticles, which mitigates pore collapse and active-site loss during repeated cycles. A gradual decline in efficiency was observed for both the hydrogel and the composite, likely due to partial pore blockage, polymer relaxation, and incomplete desorption of dye molecules [41]. Such degradation trends are commonly reported for biopolymer-based hydrogels. For example, Yue *et al.* [42] observed a decline from 95% to 70% after five regeneration cycles for an acrylamide-based hydrogel used for dye adsorption. Similarly, Chiew *et al.* [43] reported that a calcium-alginate and alginate-halloysite nanocomposite hydrogel retained ~65% efficiency after four cycles, while Wan *et al*. [44] noted that alginate immobilized TiO_2 showed improved stability compared to the neat polymer matrix due to their inorganic reinforcement.

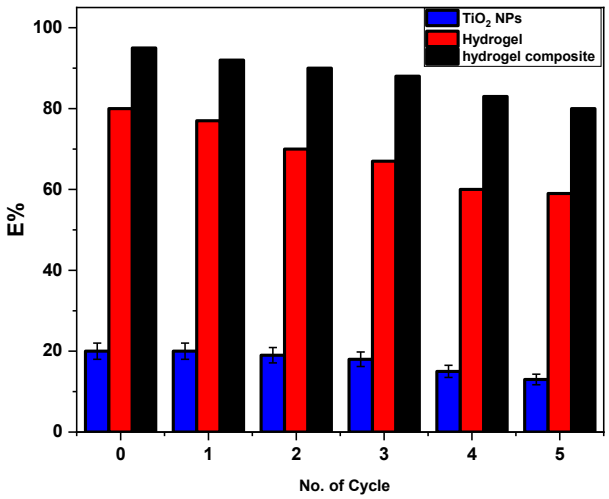

Fig. 13. Regeneration performance of TiO_2 nanoparticles, hydrogel, and hydrogel composite over five adsorption-desorption cycles (adsorption dose 0.08 g, conc. 100 mg/L, pH 7, T 25 ℃).

Compared with these systems, the SA-g-(AA-co-IA)/TiO_2 hydrogel composite reported here exhibits comparable or superior reusability, supporting its suitability for repeated wastewater treatment applications. Nonetheless, extended cycling (> 10 cycles) and structural characterization after regeneration will be required in future studies to more fully assess long-term durability [45].

IV. Adsorption Isotherm

The equilibrium adsorption of the BG dye was evaluated by fitting experimental data to the Langmuir and the Freundlich isotherm models. At a constant temperature, these models describe the relationship between the drug concentration in solution and the amount adsorbed on the SA-g-(AA-co-IA)/TiO_2 surface. Adsorption data were obtained at various initial concentrations of the BG dye (ranging from 50 to 200 mg/L). The analysis provided insights into the SA-g-(AA-co-IA)/TiO_2 maximum adsorption capacity, estimated from the applied isotherm models [46, 47].

The Langmuir model (Eq. (4)) describes homogeneous adsorption, meaning the surface has uniformly distributed active sites:

$$Q_e = \frac{Q_m K_L C_e}{1+K_L C_e} \quad (4)$$

The Freundlich model (Eq. (5)) describes a multi-layer adsorption surface that contains heterogeneous sites:

$$Q_e = K_f C_e^{\frac{1}{n}} \quad (5)$$

where Q_e: unit equilibrium adsorption efficiency (mg/g), Q_m: maximum drug uptake, providing information about adsorption efficiency for a monolayer (mg/g), C_e: concentration of drug at equilibrium (mg/L), K_L: constant denoting the energy of adsorption and affinity of the binding sites (L/mg), K_f: Freundlich constant [(mg/g)(L/mg)$^{1/n}$], n: adsorption intensity.

The absorption data for BG dye across various model equations are presented in the fitting curves shown in Fig. 14. According to the fitting data, the Freundlich isotherm model demonstrated the strongest correlation with the experimental data, as indicated by its high R^2 value of 0.9875. Thus, it suggests that adsorption occurs on a heterogeneous surface, leading to multilayer formation. The Freundlich constant 1/n is 0.612, which is greater than 1, confirming that the drug's adsorption onto the SA-g-(AA-co-IA)/TiO_2 is favourable and likely occurs via a physical mechanism rather than chemical bonding. The value of K_F for the SA-g-(AA-co-IA)/TiO_2 is 65.5 mg /g [16, 48]. These values, derived from the Freundlich model, strongly confirm that the adsorption of the BG dye onto the synthesised SA-g-(AA-co-IA)/TiO_2 is primarily a physical adsorption process, occurring on a heterogeneous surface with moderate, multilayer interactions. All parameters calculated based on the fitting of different isotherm models are provided in Table 1.

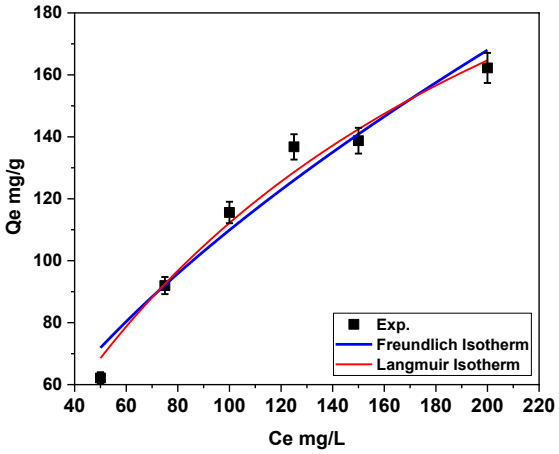

Fig. 14. Nonlinear isotherm models fit for the adsorption of the BG dye on SA-g-(AA-co-IA)/TiO_2.

Table 1. Parameters adsorption nonlinear isotherm models for the adsorption of BG dye on SA-g-(AA-co-IA)/TiO_2

Isotherm	Parameter	Value (at 25°C)
Freundlich	K_f([(mg/g)(L/mg)$^{1/n}$)	65.11±0.211
	1/n	0.612±0.0211
	R^2	0.9875
Langmuir	q_m (mg/g)	162.22±9.77
	K_L (L/mg)	0.055±0.033
	R^2	0.9234

A. Comparative Analysis with Existing Adsorbents

A comparative assessment was performed to contextualize the adsorption performance of the SA-g-(AA-co-IA)/TiO_2 hydrogel relative to previously reported materials for cationic BG dye removal. Although differences in experimental conditions across studies limit direct one-to-one comparison, the data summarized in Table 2 clearly illustrate that the synthesized hydrogel exhibits competitive and in several cases superior removal efficiency. This highlights the enhanced adsorption capability derived from the synergistic interaction between the polymer matrix and the incorporated TiO_2 nanoparticles.

Table 2. Comparative removal of dyes by hydrogel

Sorbent	Dyes	pH	T (°C)	t (hr.)	Dose (g)	Co (mg/L)	E%	Ref.
SA/CMC/TiO_2	MB	6.8	30	2	0.15	50	94.11	[49]
SA/CMC/TiO_2	CR	5	30	2	0.15	50	85.44	[49]
SA/(A-AAB)	CV	6	30	3	0.2	100	93.11	[50]
SA/bentonite clay	CV	6	30	3	0.2	100	85.01	[50]
PAM/SH/clay	MB	6.8	25	1	0.05	20	87.55	[51]
(AM-g-GO)	CR	5	30	1	0.25	50	94.4	[52]
CS/ZnO nano	CR	5	30	1	0.1	100	91.11	[49]
CS/ZnO nano	MB	6.8	30	1	0.1	100	81.33	[49]
SA-g-Poly AC	MV	7	30	1	0.3	100	86.55	[38]
SA-g-Poly AC/TiO_2	MV	7	25	1	0.3	100	98.2	[38]
SA-g-(AC-co-IA)/TiO_2	BG	7	25	1	0.08	100	91.22	In this study

B. Limitations and Future Perspectives

The present study focuses on synthesis, structural characterization, and adsorption performance evaluation of the TiO_2-reinforced hydrogel. However, the BET surface area of the pristine hydrogel was not measured under identical conditions, limiting direct comparison with the composite. In addition, detailed adsorption kinetic modeling was not performed, restricting mechanistic interpretation. Future work will include systematic surface area comparison and comprehensive kinetic and isotherm analyses to further elucidate the adsorption mechanism.

V. Conclusion

This work presents a novel SA-g-(AA-co-IA)/TiO_2 hydrogel composite that integrates a binary polyacid monomer system (acrylic acid + itaconic acid) with TiO_2 nanoparticles into a single cross-linked architecture. Unlike previously reported alginate-based hydrogels that rely on a single monomer or lack inorganic reinforcement, the current system exhibits a synergistic enhancement in swelling, structural stability, and adsorption performance. The dual-acid copolymerization provides a higher density of ionizable –COOH groups, while TiO_2 nanoparticles reinforce the polymer network and create additional dye-binding sites. This hybrid design results in superior adsorption efficiency (91.2%) and reusability compared to conventional alginate or TiO_2-based adsorbents. To the best of our knowledge, no prior study has reported a TiO_2-reinforced alginate/AA/IA hydrogel prepared via free-radical grafting for targeted removal of brilliant green dye.

Conflict of Interest

The authors declare no conflict of interest.

Author Contributions

A.M.: Supervision, Conceptualization, Methodology, Software, Validation. U.H. and H.H.: Writing- Reviewing and Editing. A.A.L.: Data curation, Writing- Original draft preparation. A.A. and W.N.: Visualisation, Investigation, A.F.: Material preparation, data collection. Finally, all authors read and approved the final manuscript.

References

[1] S. R. Shirsath *et al.*, "Ultrasonically prepared poly(acrylamide)-kaolin composite hydrogel for removal of crystal violet dye from wastewater," *J. Environ. Chem. Eng.*, vol. 3, pp. 1152–1162, 2015. https://doi.org/10.1016/j.jece.2015.04.016

[2] E. C. Silva *et al.*, "Recyclable 3D-printed composite hydrogel containing rice husk biochar for organic contaminants adsorption in tap water," *ACS Appl. Polym. Mater.*, vol. 5, pp. 8415–8429, 2023. doi.org/10.1021/acsapm.3c01534

[3] A. M. Aljeboree and A. S. Abbas, "Removal of pharmaceutical (paracetamol) by using CNT/ TiO_2 nanoparticles," *Journal of Global Pharma Technology*, vol. 11, pp. 199–205, 2019. doi: 2-s2.0-84937037071

[4] S. Sharma *et al.*, "Adsorption of cationic dyes onto carrageenan and itaconic acid-based superabsorbent hydrogel: Synthesis, characterization and isotherm analysis," *J. Hazard. Mater.*, vol. 421, 126729, 2021. https://doi.org/10.1016/j.jhazmat.2021.126729

[5] V. Tainara, S. E. S. Artifon, C. T., P. B. V., V. A. B., and A. T. P., "Chitosan-based hydrogels for the sorption of metals and dyes in water: isothermal, kinetic, and thermodynamic evaluations," *Colloid. Polym. Sci.*, vol. 299, pp. 649–662, 2021. doi.org/10.1007/s00396-020-04786-2

[6] Z. Yang *et al.*, "Carboxymethyl cellulose-based supramolecular hydrogel with thermo-responsive gel-sol transition for temporary plugging of oil pipeline in hot work," *Carbohydr. Polym.*, vol. 324, 2024. https://doi.org/10.1016/j.carbpol.2023.121556

[7] N. Ullah *et al.*, "Preparation and dye adsorption properties of activated carbon/clay/sodium alginate composite hydrogel membranes," *RSC Adv.*, vol. 14, pp. 211–221, 2024. https://doi.org/10.1039/d3ra07554k

[8] H. Al-Aidy and E. Amdeha, "Green adsorbents based on polyacrylic acid-acrylamide grafted starch hydrogels: the new approach for enhanced adsorption of malachite green dye from aqueous solution," *Int. J. Environ. Anal. Chem*, vol. 101, pp. 2796–2816, 2021. https://doi.org/10.1080/03067319.2020.1711896

[9] A. Tshikovhi and T. E. Motaung, "Chitosan and guar-gum-based polymeric nanocomposites for the adsorption of contaminants in water: Insights into adsorption capacities, mechanisms, and applications," *Desalin. Water Treat.*, vol. 320, 2024. https://doi.org/10.1016/j.dwt.2024.100708

[10] A. K. Sharma *et al.*, "Environmentally benign approach for the efficient sequestration of methylene blue and coomassie brilliant blue using graphene oxide emended gelatin/beta-carrageenan hydrogels," *Int. J. Biol. Macromol.*, vol. 219, pp. 353–365, 2022. https://doi.org/10.1016/j.ijbiomac.2022.07.216

[11] A. M. Algubili *et al.*, "Photocatalytic degradation of remazol brilliant blue dye by ZnO/UV process," *International Journal of Chemical Sciences*, vol. 13, pp. 911–921, 2015. doi: 2-s2.0-84937037071

[12] J. Irfan *et al.*, "A superabsorbent and pH-responsive copolymer-hydrogel based on acemannan from Aloe vera (Aloe barbadensis M.): A smart material for drug delivery," *Int. J. Biol. Macromol.*, vol. 270, 2024. https://doi.org/10.1016/j.ijbiomac.2024.132306

[13] S. Radoor *et al.*, "Low-cost and eco-friendly PVA/carrageenan membrane to efficiently remove cationic dyes from water: Isotherms, kinetics, thermodynamics, and regeneration study," *Chemosphere*, vol. 350, 140990, 2024. doi: 10.1016/j.chemosphere.2023.140990

[14] R. Tyagi *et al.*, "Optimization of hazardous malachite green dye removal process using double derivatized guar gum polymer: A fractional factorial L9 approach," *Sustainable Chemistry for Climate Action*, 100043, 2024. https://doi.org/10.1016/j.scca.2024.100043

[15] H. Subhan *et al.*, "Sodium alginate grafted hydrogel for adsorption of methylene green and use of the waste as an adsorbent for the separation of emulsified oil," *Journal of Water Process Engineering*, vol. 46, 2022. https://doi.org/10.1016/j.jwpe.2021.102546

[16] M. Rizwan *et al.*, "Kinetic model studies of controlled nutrient release and swelling behavior of combo hydrogel using Acer platanoides cellulose," *Journal of the Taiwan Institute of Chemical Engineers*, vol. 131, 2022. https://doi.org/10.1016/j.jtice.2021.11.004

[17] H. Subhan *et al.*, "Sodium alginate grafted poly (N-vinyl formamide-co-acrylic acid)-bentonite clay hybrid hydrogel for sorptive removal of methylene green from wastewater," *Colloids Surf. Physicochem. Eng. Aspects*, vol. 611, 2021. https://doi.org/10.1016/j.colsurfa.2020.125853

[18] B. Salunkhe and T. P. Schuman, "Super-adsorbent hydrogels for removal of methylene blue from aqueous solution: Dye adsorption isotherms, kinetics, and thermodynamic properties," *Macromol*, vol. 1, pp. 256–275, 2021. doi: 10.3390/macromol1040018

[19] H. Safarzadeh *et al.*, "Application of a novel sodium alginate-graft-poly (methacrylic acid-co-acrylamide)/montmorillonite nanocomposite hydrogel for removal of malachite green from wastewater," *J. Polym. Res.*, vol. 30, 157, 2023. doi: 10.1007/s10965-023-03531-x

[20] M. R. Xisto *et al.*, "Biopolymer gellan-gum-based TiO_2: A green alternative photocatalyst approach for removal of pollutants," *Water*, vol. 16, 2024. https://doi.org/10.3390/w16020315

[21] A. M. Aljeboree *et al.*, "Removal of textile dye (methylene blue mb) from aqueous solution by activated carbon as a model (corn-cob source waste of plant): As a model of environmental enhancement," *Plant Archives*, vol. 19, pp. 906–909, 2019. doi: 2-s2.0-85073513426

[22] S. Khan *et al.*, "Synthesis of poly (GG-co-AAm-co-MAA), a terpolymer hydrogel for the removal of methyl violet and fuchsin basic dyes from aqueous solution," *ACS Omega*, vol. 9, pp. 7692–7704, 2024. doi: 10.1021/acsomega.3c07118

[23] A. M. Aljeboree and A. F. Alkaim, "Studying removal of anionic dye by prepared highly adsorbent surface hydrogel nanocomposite as an applicable for aqueous solution," *Sci. Rep.*, vol. 14, 9102, 2024. doi: 10.1038/s41598-024-59545-y

[24] B. M. Thamer *et al.*, "Activated carbon-incorporated tragacanth gum hydrogel biocomposite: A promising adsorbent for crystal violet dye removal from aqueous solutions," *Gels*, vol. 9, 2023. doi: 10.3390/gels9120959

[25] B. M. Thamer *et al.*, "In situ preparation of novel porous nanocomposite hydrogel as effective adsorbent for the removal of cationic dyes from polluted water," *Polymers*, vol. 12, 2020. doi: 10.3390/polym12123002
[26] N. Thombare *et al.*, "Design and development of guar gum based novel, superabsorbent and moisture retaining hydrogels for agricultural applications," *Carbohydr. Polym.*, vol. 185, pp. 169–178, 2018. https://doi.org/10.1016/j.carbpol.2018.01.018
[27] M. Xinyou *et al.*, "Synthesis of a three-dimensional network sodium alginate–poly (acrylic acid)/attapulgite hydrogel with good mechanic property and reusability for efficient adsorption of Cu^{2+} and Pb^{2+}," *Environ. Chem. Lett.*, vol. 16, pp. 653–658, 2018. doi: 10.1007/s10311-018-0708-9
[28] M. Rizwan *et al.*, "Optimization of swelling and mechanical behavior of Acer platanoides cellulose combo hydrogel," *Kuwait J. Sci.*, vol. 51, 2024. https://doi.org/10.1016/j.kjs.2024.100177
[29] X. Yang *et al.*, "Novel porous hydrogel beads based on amidoxime modified polymer of intrinsic microporosity for efficient cationic dye removal," *Microporous Mesoporous Mater.*, vol. 377, 2024. https://doi.org/10.1016/j.micromeso.2024.113218
[30] E. Manaila and G. Craciun, "Poly (acrylic acid)-sodium alginate superabsorbent hydrogels synthesized by electron-beam irradiation-part II: Swelling kinetics and absorption behavior in various swelling media," *Gels*, vol. 10, 2024. https://doi.org/10.3390/gels10090609
[31] F. Amjad *et al.*, "A superabsorbent and pH-responsive copolymer-hydrogel based on glucomannans from Ocimum basilicum (sweet basil): A smart and non-toxic material for intelligent drug delivery," *Int. J. Biol. Macromol.*, vol. 315, 2025. https://doi.org/10.1016/j.ijbiomac.2025.144452
[32] P. J. Flory and J. J. Rehner, "Statistical mechanics of cross-linked polymer networks I. Rubberlike elasticity," *J. Chem. Phys.*, vol. 11, pp. 512–520, 1943. doi: 10.1063/1.1723791
[33] J. Wei *et al.*, "Carbon nanotube/chitosan hydrogel for adsorption of acid red 73 in aqueous and soil environments," *BMC Chemistry*, vol. 17, 104, 2023. doi: 10.1186/s13065-023-01019-9
[34] B. Vahid *et al.*, "Synthesis and characterization of bio-nanocomposite hydrogel beads based on magnetic hydroxyapatite and chitosan: A pH-sensitive drug delivery system for potential implantable anticancer platform," *Polymer Bulletin*, vol. 23, 1223, 2023. https://doi.org/10.1007/s00289-023-05072-1
[35] A. M. Aljeboree *et al.*, "Highly reusable nano adsorbent based on clay-incorporated hydrogel nanocomposite for cationic dye adsorption," *J. Inorg. Organomet. Polym. Mater.*, vol. 35, pp. 1165–1186, 2025. https://doi.org/10.1007/s10904-024-03344-5
[36] Y. Zhao *et al.*, "Preparation of SA-g-(PAA-co-PDMC) polyampholytic superabsorbent polymer and its application to the anionic dye adsorption removal from effluents," *Sep. Purif. Technol.*, vol. 188, pp. 329–340, 2017. https://doi.org/10.1016/j.seppur.2017.07.044
[37] Z. Wang *et al.*, "Synthesis and swelling behaviors of carboxymethyl cellulose-based superabsorbent resin hybridized with graphene oxide," *Carbohydr. Polym.*, vol. 157, pp. 48–56, 2017. doi: 10.1016/j.carbpol.2016.09.070
[38] S. Thakur and O. Arotiba, "Synthesis, characterization and adsorption studies of an acrylic acid-grafted sodium alginate-based TiO_2 hydrogel nanocomposite," *Adsorption Science & Technology*, vol. 36, pp. 458–477, 2018. doi: 10.1177/0263617417700636
[39] M. Zheng *et al.*, "pH-responsive poly (gellan gum-co-acrylamide-co-acrylic acid) hydrogel: Synthesis, and its application for organic dye removal," *Int. J. Biol. Macromol.*, vol. 153, pp. 573–582, 2020. https://doi.org/10.1016/j.ijbiomac.2020.03.024
[40] N. A. Elessawy *et al.*, "Novel sodium alginate/polyvinylpyrrolidone/TiO_2 nanocomposite for efficient removal of cationic dye from aqueous solution," *Appl. Sci.*, vol. 11, 9186, 2021. doi: 10.3390/app1119918
[41] U. A. R. Hussein *et al.*, "Green adsorbents for pharmaceutics removal from aqueous solution: Regeneration and reused for environmental study," *Procedia Environmental Science, Engineering and Management*, vol. 12, pp. 229–235, 2025. doi: 2-s2.0-105007606095
[42] Y. Yue *et al.*, "Highly recyclable and super-tough hydrogel mediated by dual-functional TiO_2 nanoparticles toward efficient photodegradation of organic water pollutants," *J. Colloid Interface Sci.*, vol. 564, pp. 99–112, 2020. https://doi.org/10.1016/j.jcis.2019.12.069
[43] C. C. Chiew *et al.*, "Stability and reusability of alginate-based adsorbents for repetitive lead (II) removal," *Polym. Degrad. Stab.*, vol. 123, pp. 146–154, 2016. https://doi.org/10.1016/j.polymdegradstab.2015.11.022
[44] S. Wan *et al.*, "Novel alginate immobilized TiO_2 reusable functional hydrogel beads with high photocatalytic removal of dye pollutions," *Journal of Polymer Engineering*, vol. 42, no. 10, pp. 978–985, 2022. doi:10.1515/polyeng-2022-0017
[45] F. Bessaha *et al.*, "Characterization and application of heat-treated and acid-leached halloysites in the removal of malachite green: adsorption, desorption, and regeneration studies," *Desalin. Water Treat.*, vol. 57, pp. 14609–14621, 2016. https://doi.org/10.1080/19443994.2015.1063090
[46] B. K. Martini *et al.*, "Methyl orange and tartrazine yellow adsorption on activated carbon prepared from boiler residue: Kinetics, isotherms, thermodynamics studies and material characterization," *J. Environ. Chem. Eng.*, vol. 6, pp. 6669–6679, 2018. https://doi.org/10.1016/j.jece.2018.10.013
[47] J. Parlayici and A. Aras, "Synthesis of a novel green biopolymer-based composites beads for removal of methylene blue from aquatic medium: Isotherm, thermodynamic and kinetic investigation," *Polym. Bull.*, vol. 81, pp. 6603–6640, 2024. https://doi.org/6610.1007/s00289-00024-05164-00286
[48] P. Kumari *et al.*, "Synthesis of gum acacia-cl-acrylic acid-co-itaconic acid hydrogels for efficient removal of toxic dye rhodamine-B: A step for sustainable environment," *Int. J. Biol. Macromol.*, vol. 292, 2025. https://doi.org/10.1016/j.ijbiomac.2024.139296
[49] M. T. Alsamman and J. Sánchez, "Recent advances on hydrogels based on chitosan and alginate for the adsorption of dyes and metal ions from water," *Arab. J. Chem.*, vol. 14, 202112, 2021. doi: 10.1016/j.arabjc.2021.103455
[50] A. A. Oladipo and M. Gazi, "Enhanced removal of crystal violet by low cost alginate/acid activated bentonite composite beads: Optimization and modelling using non-linear regression technique," *Journal of Water Process Engineering*, vol. 2, pp. 43–52, 2019. https://doi.org/10.1016/j.jwpe.2014.04.007
[51] J. Z. Yi and L. M. Zhang, "Removal of methylene blue dye from aqueous solution by adsorption onto sodium humate/polyacrylamide/clay hybrid hydrogels," *Bioresour. Technol.*, vol. 99, pp. 2182–2186, 2008. https://doi.org/10.1016/j.biortech.2007.05.028
[52] H. S. Al-Niaeem *et al.*, "Preparation of semi IPNs-hydrogel composite for removing congo red and bismarck brown Y from wastewater: Kinetic and thermodynamic study," *Egypt. J. Chem.*, vol. 56, pp. 19–34, 2022. doi: 10.21608/ejchem.2021.66511.3438